Applied Surface Science 675 (2024) 160962

Contents lists available at ScienceDirect

Applied Surface Science

journal homepage: www.elsevier.com/locate/apsusc

Full Length Article

Evidence as conformational molecular switch of 1,4-bis(4-vinylpyridyl) benzene adsorbed on a nanostructured silver surface: A synergetic study of femtosecond transient absorption spectra, electrochemical SERS records and DFT calculations

Isabel López-Tocón [a,*], Miguel García-Castro [b], Juan Carlos Otero [a]

[a] Andalucía Tech, Departamento de Química Física, Facultad de Ciencias, Universidad de Málaga, Málaga, Spain
[b] Andalucía Tech, Departamento de Química Orgánica, Facultad de Ciencias, Universidad de Málaga, Málaga, Spain

ARTICLE INFO

Keywords:
SERS spectroscopy
Transient absorption spectroscopy
TD-DFT calculations
1, 4-bis(4-vinylpyridyl)benzene

ABSTRACT

The electrochemical surface-enhanced Raman spectra (SERS) of 1,4-bis(4-vinylpyridyl)benzene (bvpb) recorded at different electrode potentials with three excitation wavelengths (785, 532 and 473 nm) point out there exists a resonance process involved at more negative voltage with the 785 nm line, giving two strongly enhanced SERS bands at about 1500 and 1150 cm^{-1}. This result agrees with the VIS-NIR transient absorption spectrum characterized by a strong band at 607 nm and a weaker one at 1163 nm, corresponding to the first singlet (S_1) and triplet (T_1) excited electronic states. The DFT potential energy curve corresponding to the *trans–cis* (*E-Z*) isomerization in the S_0 state and in the two lowest S_1 and T_1 excited states, indicates that the S_1 state exhibits a significant lower barrier height than S_0 state, showing also a S_1/S_0 conical intersection at a structural conformation in which the vinyl double bond twists by 90°. TD-DFT resonance Raman spectra of the planar and twisted conformation in a simple model of surface complex, Ag_2^0-bvpb, yield that the twisted molecule is able to predict the selected enhancement of the two SERS bands. Therefore, bvpb could act as an electroactive conformational molecular switch under a selected wavelength in nanoelectronic devices.

1. Introduction

The photochemical *cis–trans* (*Z-E*) isomerization of organic molecules with a double bond in their structure have been widely studied because this process plays a main role in many photoreceptive biological functions such as vision and phototaxis [1,2] or the vitamin D production [3], as well as, in devices that use photoisomerizable additives/pigments to change their properties such as, rewritable CDs, DVDs, 3D optical data storage and liquid crystals. Nowadays, the interest in photoisomerizable molecules has been aimed at new functional materials and molecular devices, such as molecular switches [4], molecular motors [5] and molecular electronics [6].

One prominent type of compounds subject to photoisomerism are stilbenes [7,8] and related heterocyclic analogues (heterostilbenes) [9,10]. The photochemistry of stilbene has attracted considerable attention and interest for researchers [7,11–15] and has been extensively investigated from experimental [7,11–16] and computational [15,17–20] point of view, being addressed in two ways: the elucidation of which mechanism, hula-twist or one-bond flip [1,7], is involved in the *Z-E* isomerization and the detection of the transient species in the first excited electronic state, S_1, corresponding to a perpendicular molecular geometry, when one of the benzene rings is rotated by 90° around the vinyl bond [13,14]. This is a common intermediate between the two excited *trans*- and *cis*-species, being called the phantom state due to its difficulty to be detected and its short lifetime.

The transient absorption spectroscopy (TAS) with time-resolution in femtoseconds gets insight into the nature and dynamics of relaxation processes in the transient species. The main conclusions related to the photoreactivity and excited states of *trans*- and *cis*-stilbenes [7,13,14] can be summarized as follows, the hula-twist mechanism can take place not only in a fluid medium but also in free molecules without any constraint [7] and, the lifetime of the phantom state was found to be around 135–160 fs [13], while those of the singlet excited *trans* and *cis* species are 10 to > 100 ps [16], depending of the excess of energy, and

* Corresponding author at: Andalucía Tech, Departamento de Química Física, Facultad de Ciencias, Universidad de Málaga, Málaga, Spain.
E-mail address: tocon@uma.es (I. López-Tocón).

https://doi.org/10.1016/j.apsusc.2024.160962
Received 23 May 2024; Received in revised form 15 July 2024; Accepted 10 August 2024
Available online 12 August 2024

300 fs [21,22], respectively. From computational point of view, most of the works [17,23–25] conclude that the majority of *E-Z* photoisomerization reactions involved in the S_1 state proceed via a conical intersection (CI) between the S_1 and S_0 states, whereas a crossing to the triplet (T_1) excited states rarely occurs due to a large energy gap between the corresponding singlet and triplet excited states.

Nonetheless, although the TAS spectra provide information on the electronic transitions of the excited states created by the photoexcitation, no information on the structural changes that a molecule suffers in the excited state can be extracted. Concerning the photoexcitation of stilbene, no experimental evidences of the rotation by 90° of the double bond in the S_1 state, and thus a perpendicular molecular geometry in the phantom state, were shown by any time-resolved vibrational spectroscopy [26], due to the low temporal and spectral resolution of this technique. To this regard, surface-enhanced Raman scattering (SERS) [27] could be a complementary spectroscopic tool to TAS spectra because it is a vibrational technique that allows us to extract information on the molecular electronic structure and even, on the changes in the molecular conformation upon excitation [28], with the help of theoretical calculations. This technique is mainly characterized by a selective enhancement of the bands of an aromatic molecule adsorbed or close to a nanostructured metal, as a consequence of a resonance process between the ground electronic state (S_0) and an excited electronic state of the adsorbate [29] or the metal-adsorbate hybrid that shows charge-transfer (CT) characteristics [30]. In electrochemical SERS experiments, the resonance condition can be reached under visible excitation line at negative electrode potential [28,30–32] yielding information on the molecular conformation in such excited electronic state.

In this work, a synergy of experimental, TAS and SERS spectra, and computational results is provided to investigate the effect of *E-Z* photoisomerization process of a double heterostilbene, 1,4-bis(4-vinylpyridyl)benzene, adsorbed on a nanostructured silver surface, hereinafter be called bvpb. This molecule shows two end pyridines connected each one by a vinyl bond to a central benzene ring. Because of its photoinduced molecular isomerization reaction could be analogue to that of stilbene, bvpb can play an important role in the optoelectronic field and also, in the design of new functional materials by acting as a building block in three-dimensional supramolecular self-assembling compounds [33] at metal surfaces and interfaces, due to the presence of the two nitrogen atoms in the two end pyridines.

The investigation follows several steps: firstly, bvpb was synthesized and characterized by experimental techniques and DFT calculations. Its electronic structure and the *E-Z* photoisomerization process were investigated by TAS technique and DFT calculations related to the potential energy curve of a vinyl torsion. Then, the adsorption of bvpb on silver surface was investigated by electrochemical SERS spectra and also DFT calculations applied to a series of simple linear metal-(*E,E*)-bvpb complexes, Ag_n^q-(*E,E*)-bvpb, with different sizes (n) and charges (q) that allows to simulate the effect of the electrode potential on the electronic structure of adsorbed bvpb. In addition, the conventional Raman and resonance Raman of bvpb isolated and complexed were also calculated and compared with the experimental ones.

This study allows us to conclude from TAS data that the photoexcitation of bvpb in aqueous solution decays to the S_0 state in a radiationless ultrafast process through S_0/S_1 CI. There exists a competitive process related to an intersystem crossing practically from the Franck-Condon point to the CI given that the two TAS bands, at 607 nm (2.04 eV) and 1163 nm (1.07 eV), corresponding to the S_1 and T_1 excited states, show a similar dynamics of relaxation, and thus, the electronic state is degenerated in such region due to a common molecular conformation for the two states. This behaviour is corroborated by DFT calculations, which yield a geometry with the vinylpyridil group twisted at 90° as a responsible of the degenerated electronic state. A similar twisted geometry could be involved in the strong enhancement of two SERS bands, about 1500 and 1150 cm^{-1}, observed in the electrochemical SERS experiments at negative electrode potential, −1.0 V, with 785 nm (1.58 eV) excitation line, due to the close proximity to the S_1 state resonance (2.04 eV). In fact, the resonance Raman spectra calculated for the twisted molecule by using a simple model of surface complex, Ag_2^0-bvpb, is able to explain the enhancement of these two bands while an all-*trans* planar structure cannot support the experimental evidence. SERS experiments also show that the S_1 state, and thus a twisted geometry, can be tuned by the electrode potential in a reversible way without molecular damage, what allows us to conclude that bvpb could be employed as conformational molecular switch addressed by electric potential under a selected wavelength.

2. Material and methods

2.1. Synthesis and characterization of 1,4-bis(4-vinylpyridyl)benzene, (bvpb)

All reagents of the available highest purity were purchased from Aldrich chemicals. A similar synthetic procedure to that previously reported [34] was performed. Briefly, benzoyl chloride (4.96 mL, 43 mmol, 2.0 equiv.) was slowly added to a solution of 4-methylpyridine (4.18 mL, 43 mmol, 2.0 equiv.) in DMF (50 mL) at room temperature. After stirring for 30 min, a solution of terephthaldicarboxaldehyde (2.88 g, 21.5 mmol, 1.0 equiv.) in DMF (20 mL) was then added and the reaction mixture heated under reflux for 12 h. The resulting solution was cooled to room temperature and poured into water–ice (300 mL) which was rendered basic by addition of ammonia until pH=10–12. The crude product was collected by filtration and washed with solution of HCl 2 M, yielding the corresponding dihydrochloride dipyridinium salt of bvpb as a yellow solid (25 % yield in two steps), **m.p:** 309–319 °C; **Elemental analysis**: C, 61.5 %; H, 5.4 %; N, 7.3 %. ($C_{20}H_{16}N_2$•2HCl requires C, 67.2 %; H, 5.1 %; N, 7.8 %; Cl, 19,8 %); **^{1}H NMR (400 MHz, D_2O), δ (ppm):** 8.33 (d, 4H, *J*=6.8 Hz), 7.74 (d, 4H, *J*=6.8 Hz), 7.33 (s, 4H), 7.21 (d, 2H, *J*=16.3 Hz), 6.83 (d, 2H, *J*=16.3 Hz); **^{13}C NMR (100 MHz, D_2O), δ (ppm):** 154.6, 140.4, 139.3, 136.4, 128.8, 123.4, 123.3. **UV Absorption:** 370 nm. **Raman spectrum** (excitation line λ = 785 nm): three strong bands at 1625, 1596 and 1178 cm^{-1} assigned to in-plane modes; ethylene C═C bond stretching, C—C bond stretching (8a mode) and C—H bending of central benzene ring, respectively.

2.2. Instrumentation

A TruSpec Micro elemental analyzer (Leco, USA) was employed in carbon, hydrogen and nitrogen determination, being able to perform measurements in small samples (2.5 mg). An Agilent 8453 UV–visible spectrometer (Agilent, USA) and a 400 Plus Avance III spectrometer (Bruker, USA) were used for recording the absorption spectrum in aqueous solution and the NMR spectra, respectively.

The Raman and SERS spectra were recorded by a Renishaw InVia Qontor micro-Raman spectrometer (Renishaw, UK) with 1 cm^{-1} spectral resolution using three exciting lines, 785, 532 and 473 nm. An adapted objective (f:30 mm) was used to work in macro conditions. The laser power at the sample was 5–10 mW, depending of the excitation wavelength, and Wire 2.0 software (Renishaw) was used for spectral acquisition and manipulation. A single scan and 10 s exposure time were selected to avoid sample damage. The sequence of spectra was recorded twice to check that the relative intensity of the bands kept constant.

An electrochemical cell composed by three electrodes, a platinum counter electrode, an Ag/AgCl/KCl (sat) reference electrode and a pure silver working electrode was employed for recording spectroelectrochemical SERS experiments. The silver surface was polished with 0.30 alumina (Büehler, USA) and then electrochemically activated by an oxidation–reduction pre-treatment involving seven pulses of a triangular sweep from −0.5 V to + 0.6 V at 5 mV/s using a 0.1 M KCl aqueous solution. A potentiostat model 600E (CH Instruments Inc., USA) controls the electrode potentials. SERS spectra of bvpb/KCl aqueous solution (0.1 mM/0.1 M) were recorded in forward and reverse way, that is, from

0.0 V up to −1.4 V by step of −0.1 V and then get back to 0.0 V in the same way. This procedure was repeated twice in order to check the reproducibility.

A Helios spectrometer (Spectra Physics, USA) in a probe-reference mode was employed for recording the transient absorption spectra (TAS). However, a complete system requires a solid-state amplifier (Spitfire Ace Model F, Ti:Sapphire, 800 nm, ≤ 1KHz) that operates in a chirped pulse amplification. It also needs a pump laser (Empower, Nd-YLF, 527 nm, 1KHz), to energize the Spitfire amplifier, and a seed laser (Mai Tai, Ti:Sapphire, 800 nm, 80 MHz) to provide the original pulses. Small fraction (about 1–3 mJ) of pump pulses at 800 nm wavelength is used to produce white-light continuum in a sapphire plate inserted in the TOPAS equipment (290–1600 nm), a two-stage optical parametric amplifier. Once TOPAS is properly adjusted and calibrated the wavelength can be easily changed using WinTOPAS software and the pump beam for the specific sample can be selected. In our case, it was set at 370 nm. The other branch of the amplified 800 nm light is focused on a calcium fluoride plate or a different substrate (proprietary information of Spectra Physics) for generating a white-light continuum in the VIS and the NIR, respectively. The resulting beam is used as a broadband probe. Then, the probe is focused on the sample spatially overlapped with the pump that is set at the magic angle (54.7°) to prevent the dipole–dipole interactions between the excited molecules and the probe light.

The probe-reference mode, in which the probe beam is split into two before passing through the sample and one leg is sent to the reference spectrometer, allows to monitorize the fluctuations in the probe beam intensity. This has the advantage to achieve a good signal/noise ratio with lower number of averaged laser pulses, being of interest for photodegradable samples where the number of lasers shots is very limited. A spectral resolution of 1.5 and 3.5 nm is achieved in the VIS and NIR region. The intrinsic temporal resolution is 7 fs. An aqueous sample solution, 10^{-3} M, in a static cell with 0.2–1 mm thick quartz window and 2 mm optical pathlength was employed. The transient absorption measurements cover the 450–800 nm and 800–1600 nm spectral ranges and a 0–5 ns time range. Different times delay between the pump and probe were performed. TAS spectra were analyzed with Surface Explorer program, version 4.0.

All equipments stay in the central research support services (SCAI center) of the University of Málaga.

2.3. Theoretical calculations

Density Functional Theory (DFT) [35] was employed to calculate the equilibrium geometry, the vibrational wavenumbers and the internal rotation potential energy curve along the single C—C bond of pyridine and the double C═C ethylene bond in the S_0 state. The calculations performed in S_1 and T_1 excited states were carried out by spin-unpolarized and spin-polarized Time-Dependent DFT (TD-DFT).

Three hybrid functionals, B3LYP [36], wB97XD [37] and CAM-B3LYP[38], with the electronic basis set, 6–31+G* [39] were selected, together with the CAM-B3LYP/Def2TZVPP [38,40] level of calculation, in order to investigate the effect of the functionals and the electronic basis set on different issues such as, optimized geometrical parameters, vibrational wavenumbers, absorption band, Raman spectrum and electronic structure of bvpb. CAM-B3LYP/6–31+G* level was only employed for the potential energy curves associated with torsions of both pyridine groups with respect to the plane of the vinylene linkage and of the C═C ethylene bond implicated in the *E-Z* isomerization of bvpb, since it represents a good compromise between the quality of the results and the required computer time, as will see later.

In addition, a simple model of linear metal-(*E,E*)-bvpb complexes, Ag_n^q-(*E,E*)-bvpb, with different sizes (n) and charges (q) such as, n = 0 with q = 0 and n = 3, 5, 7 with q=±1, was employed to investigate the effect of the electrode potential on the electronic structure of bvpb adsorbed on silver surface. The combined variable $q_{eff} = q/n$ models the change of the excess of charge of a surface atom of the electrode under applied voltage [41,42]. This theoretical model yields results in agreement with the experimental evidences [41,42]. The neutral complex, Ag_2^0-(*E,E*)-bvpb, was selected to calculate the potential energy curve due to the torsion of vinyl bond and the resonance Raman spectra. This closed-shell molecular system reproduces quite well the SERS spectra in aromatic molecules [28,30,43]. Due to the presence of the silver atoms, all calculations of the surface complexes were performed at CAM-B3LYP/Def2TZVPP level.

The bulk aqueous solvent effect was also incorporated in the calculations of the isolated molecule and the metallic complex by using the polarizable continuum model (PCM=water).

Raman intensities were computed in the Born-Oppenheimer approach using the Placzek approximation [44,45]. Under these conditions, the mathematical expression for the resonance Raman cross section of a vibrational mode *p* for a perpendicular plane-polarized light becomes:

$$\left(\frac{d\sigma}{d\Omega}\right)_p = \frac{\pi^2}{\varepsilon_0^2}\left(\widetilde{\upsilon}_{in} - \widetilde{\upsilon}_p\right)^4 \frac{h}{8\pi^2 c\widetilde{\upsilon}_p} \frac{45a_p^2 + 7\gamma_p^2}{45\left[1 - \exp\left(-\frac{hc\widetilde{\upsilon}_p}{k_B T}\right)\right]}$$

Being $\widetilde{\upsilon}_{in}$ and $\widetilde{\upsilon}_p$, the wavenumbers of the incident radiation (785 nm) and of the vibrational normal mode *p*; ε_0 the vacuum permittivity; *h* the Planks constant; *c* the speed of light; k_B Boltzmann's constant and *T* the temperature. The $(45a_p^2 + 7\gamma_p^2)$ term is the Raman activity, a_p is the mean isotropic polarizability and γ_p is the derivative of the anisotropic polarizability.

Raman and UV spectra were plotted using a lorentzian function with a value of 10 units as a full width at half maximum. The computed vibrational normal modes and molecular orbitals were visualized with MOLDEN program [46]. All calculations were carried out with the GAUSSIAN16 revision C.02 program [47] provided by the Supercomputing and Bioinnovation Center (SCBI) of the University of Málaga.

3. Results and discussion

3.1. Equilibrium geometry in S_0 state and electronic structure of bvpb. Raman and UV spectra. Comparison of DFT results

The molecular geometry of bvpb was first optimized considering that the pyridine and benzene rings and the vinylene linkage are coplanar in all-*trans*-conformation (*E,E*-isomer), i.e., constrained to a C_{2h} symmetry. Due to the absence of experimental data about the structure of bvpb, the geometrical parameters calculated at different DFT levels (Table S1) were compared with the experimental data obtained in a related molecule like *trans*-stilbene [48–51].

The four levels of calculation yield values of distance and bond angles in the same order of the experimental data for *trans*-stilbene, except the calculated C—N distance, R(C4-N5), and H-$C_{ethylene}$-C_{ring} angle, A(H-C1-C2) in bvpb, that are slightly smaller (e.g. 1.339 Å and 114.3° at B3LYP/6–31+G*) than the respective C—C distance and angle in *trans*-stilbene (1.369 Å and 121.1°) [48,49]. However, some differences among the DFT calculations were detected. B3LYP/6–31+G* level gives slightly higher values of bond distances of the carbon skeletal (e.g. 1.351 Å for C=C distance) than the rest of the calculations (e.g. 1.341 Å for CAM-B3LYP/6–31+G*), while the higher level of calculation CAM-B3LYP/Def2TZVPP yields smaller values (e.g. 1.332 Å for C═C distance), as expected for a long-range-corrected functional with a huge basis set. The two functionals wB97XD and CAM-B3LYP with the same basis set, 6–31+G*, yield similar results (e.g. 1.342 Å and 1.341 Å for C═C distance), intermediate values between those of B3LYP/6–31+G* and CAM-B3LYP/Def2TZVPP. There are no other appreciable differences for the rest of parameters at any level of calculation.

The similar geometrical data between those calculated for (*E,E*)-bvpb

and those experimental for *trans*-stilbene indicate that bvpb would show an analogous geometrical structure to *trans*-stilbene. Because of *trans*-stilbene has the two phenyl rings slightly twisted by 3-7° with respect to the vinylene plane, as shown experimentally [48,49], it would be also expected an almost planar geometry for bvpb in the S_0 electronic state. In fact, the optimized structure of bvpb under a C_{2h} symmetry at any level of calculation, except at wB97XD/6–31+G* level, yields real wavenumbers, indicating an absolute equilibrium minimum. Because of the structure optimization at wB97XD/6–31+G* level gives a geometry with the two pyridine rings slightly twisted, the potential energy curves related to torsions of both pyridine rings will be investigated in the next section. As a result in advance, a flat minimum was found in a small rotational angles range in S_0 state.

Regarding to the vibrational wavenumbers, although those all calculated are overestimated with respect to the experimental ones, the theoretical Raman spectrum of (*E,E*)-bvpb at any level of calculation reproduces quite well the experimental intensities profile (Figure S1); a very strong band recorded at 1596 cm^{-1} assigned to 8a:ν_{ring} mode of the three aromatic rings and two strong bands recorded at 1625 and 1178 cm^{-1} assigned to C=C stretching and benzene C—H in-plane deformation, respectively. All recorded bands belong to a totally symmetric irreducible representation (Table S2). Only the intensities of the two bands recorded in the 1600 cm^{-1} region are swapped in the wB97XD/6-31+G* Raman spectrum (Figure S1), predicting the strongest band as that at higher wavenumber assigned to C=C stretching. Given that (*E,E*)-bvpb is a double heterostilbene, the assignment of the Raman bands has been done by correlation with those reported for *E*-stilbene (Table S2 and references in Material Supplementary).

Regarding to the electronic structure of (*E,E*)-bvpb (Table S3), each level of calculation shows a different distribution of the first ten singlet excited states according to their irreducible representations. In any case, all calculations predict a low-lying bright singlet S_1 state, 3.1 eV at B3LYP/6–31+G* and about 3.6 eV at CAM-B3LYP/6–31+G* and Def2TZVPP, that belongs to B_u irreducible representation with an oscillator strength about 1.7 arbitrary units (a.u.) at any level of calculation. This S_1 state corresponds to a π-π* transition involving the HOMO-LUMO orbitals (inset of Fig. S2a). The experimental UV spectrum and those calculated at different levels were plotted in Fig. S2a and S2b, respectively. Experimentally, an absorption band centered at 370 nm is shown (Fig. S2a), while the calculated UV band in gas phase is blue- or red-shifted about 30 nm in both cases, depending on the level of calculation (Fig. S2b), that is, the levels of calculation subestimate or overestimate the energy of the electronic states as much as a 8 % respect to the experimental value. Due to most of selected levels gives a blue-shifted UV band (−30 nm) and only the B3LYP/6–31+G* level predicts a red-shifted UV band (+30 nm), the CAM-B3LYP/6–31+G* level was chosen to study the potential energy associated with torsion of pyridine ring and of vinyl bond. This level of calculation has a good compromise between the quality of the results and the required computer time. In addition, the incorporation of the bulk solvent effect at this level of calculation by using PCM predicts an absorption band at 370 nm (Fig. S2b), in agreement with the experimental evidence.

3.2. *Torsional potential energy curves of pyridyl ring and of vinyl double bond in isolated bvpb*

Two types of torsional motion can be considered in (*E,E*)-bvpb molecule, one along the C–C single bond connecting the pyridine rings, defined by the dihedral angle ϕ, and other along the C=C double bond, defined by the dihedral angle τ. Fig. 1 shows the CAM-B3LYP/6–31+G* potential energy curves related with the torsion of the two pyridine rings leaving coplanar the benzene ring and the two double bonds. Under this

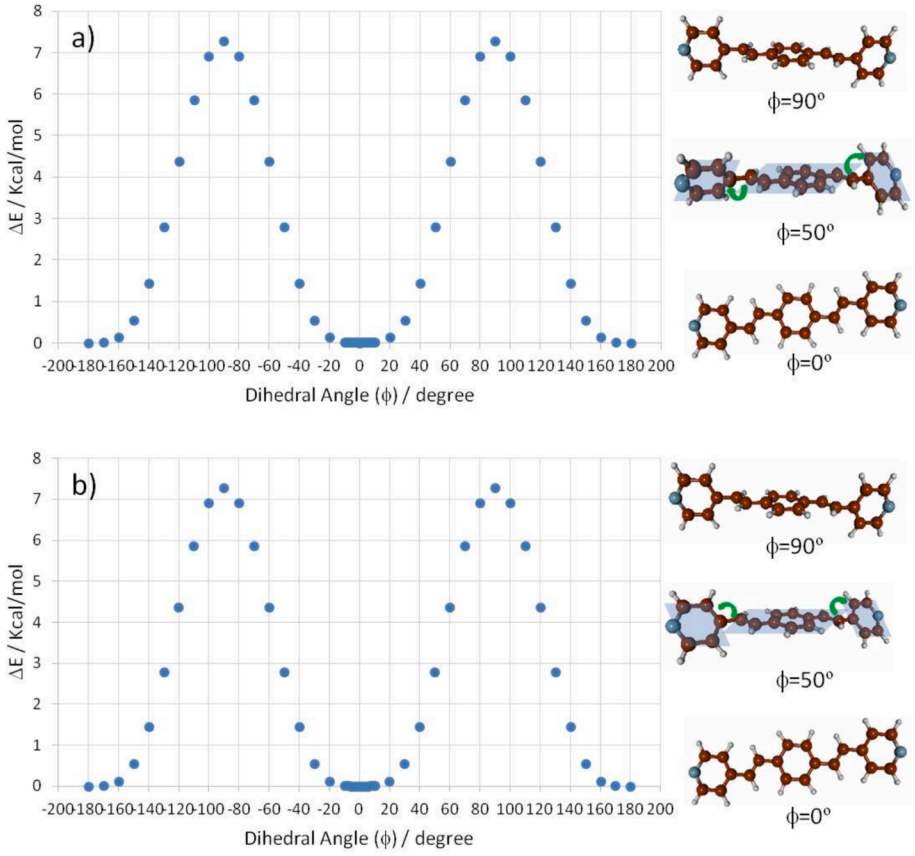

Fig. 1. Potential energy curves at CAM-B3LYP/6–31+G* level associated with torsions of both pyridine rings with respect to the plane defined by the benzene ring and the C=C double bonds (ϕ dihedral angle), keeping either C_2 (a) or C_i (b) symmetry in the structure of bvpb.

restricted condition, all geometrical parameters are optimized at each fixed ϕ angle. Both rings can be rotated by an equal amount in opposite direction leading to C_2 symmetry (Fig. 1a), or in the same direction becoming C_i symmetry (Fig. 1b). The shapes of both potential curves are very similar one each other. In both cases, the barrier for the perpendicular rings was reached at 7.3 kcal/mol in gas phase (or 9.4 kcal/mol, PCM), being in the same order of magnitude that in the case of *trans*-silbene [49] and other polyenes [52]. Also, a flat minimum between −20° and + 20° was calculated in agreement with the gas-phase electron diffraction data obtained for *trans*-stilbene that give a dihedral angle of about 30° [50]. However, the optimized C_i and C_2 conformations only differ + 0.053 and + 0.046 kcal/mol in gas phase (or + 0.012 and + 0.019 kcal/mol, PCM) with respect to the planar C_{2h} symmetry. The calculated energy difference between the C_2 and C_i symmetries is very small, ($7.2 \bullet 10^{-3}$ kcal/mol, gas phase; $6.6 \bullet 10^{-3}$ kcal/mol, PCM), being the C_2 symmetry conformation slightly more stable than C_i one in gas phase while a reverted behaviour is found in aqueous solvent. Thus, such low barrier height points out that bvpb is slightly flexible as happens in many conjugated molecules [53].

Because of two pyridine rings can act as a free rotor, the potential energy curve associated with the torsion of C=C double bond has been calculated for only one of the two vinyl bonds keeping planar the rest of the molecular structure and leaving free the ϕ angle corresponding to the rotation of pyridine ring. This implies a hula-twist mechanism in which the rotation of the C=C double and C–C single bond was involved as already evidenced in previous work [7]. Although this is the dominant photochemical reaction pathway for polyenes, a small diene or a longer polyene chromophore imbedded in a rigid medium or in a protein binding cavity such as those of rhodopsin [1] and previtamin D [54], the hula-twist can also take place in free molecules without any constraint [7], while the conventional one-bond-flip process is the preferred reaction pathway in a fluid medium [55].

Fig. 2 shows the CAM-B3LYP/6–31+G* relative potential energy profile of the ground state (S_0), and the first excited triplet (T_1) and singlet (S_1) states in gas phase by considering the rotation of one vinyl bond. The barrier of (*E,E*)-(*E,Z*) isomerization along the S_0 potential curve is 3.17 eV (+73.21 kcal/mol) with a transient state (TS) at τ = 90° and the difference energy between the two isomers, (*E,E*) and (*E,Z*), is only 0.34 eV (+7.91 kcal/mol). These values slightly change when all geometrical parameters are optimized. Figure S3 shows a potential energy diagram showing the optimized structures and energies associated with each conformer, as well as, the minimum energies required to reach the different TS. In this case, the difference energy between the (*E,E*) and (*E,Z*) isomers becomes smaller, 0.18 eV (+4.27 kcal/mol) while the barrier height, TS1, remains practically unchanged, 3.16 eV (+73.10 Kcal/mol). Also, a second isomerization, from (*E,Z*) conformation to (*Z, Z*) one, related to the other C=C double bond is considered. The barrier height (*E,Z*)-(*Z,Z*), TS2, is slightly higher (+84.29 kcal/mol) and the all-*cis*-isomer (*Z,Z*-bvpb) differs only + 4.19 and + 8.46 kcal/mol with respect to the (*E,Z*) and (*E,E*) isomers, respectively. The calculated N…N distance and ϕ angle of bvpb are the two geometrical parameters that significantly change with the isomerization (Figure S3). The N…N distance is shortened from 16.2 Å in (*E,E*) isomer to 14.2 Å in TS1 and reaches 12.7 Å in (*E,Z*) isomer, while the ϕ angle is rotated from 0° in (*E, E*) to 4.7° in TS1 and up to 40.3° in (*E,Z*) isomer. PCM calculations (orange values in Figure S3) yield similar results to that obtained previously in gas phase for the barrier heights, TS1 (+72.94 kcal/mol) and TS2 (+84.43 kcal/mol), and for the energy differences of the *cis*-isomers, (*E,Z*) and (*Z,Z*), with respect to the all-*trans* (*E,E*) one (+5.08 and + 10.14 kcal/mol, respectively). Also, the geometrical parameters, N…N distance and ϕ angle, practically are not affected by the presence of aqueous solvent (Figure S3) as also happen for the potential energy curve associated with the torsion of the vinyl bond (Figure S4) in S_0 state. In summarize, because of this high barrier along the S_0 energy, the

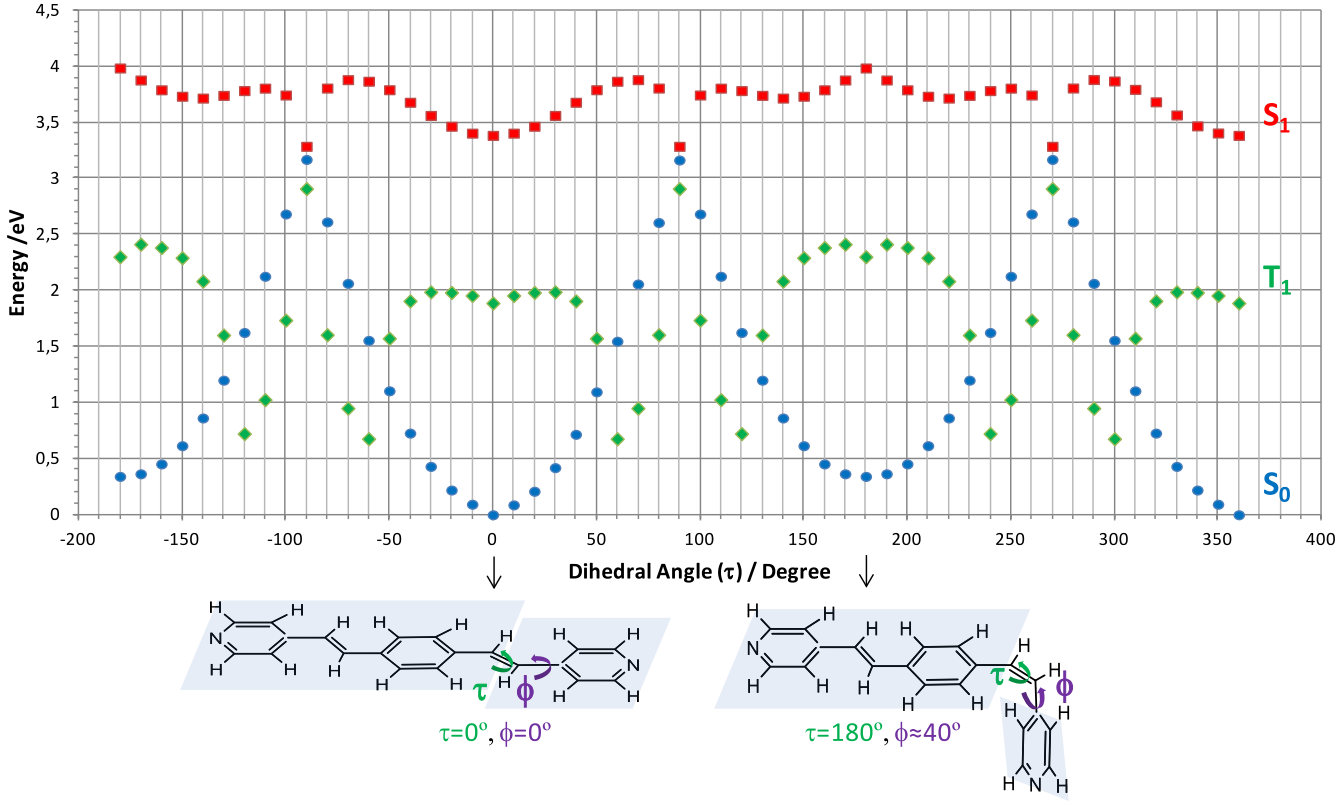

Fig. 2. CAM-B3LYP/6–31+G* potential energy curves associated with torsion of one of C=C vinyl bond according to a hula-twist mechanism in the ground electronic state (S_0) and the first excited triplet (T_1) and singlet (S_1) states. The ϕ angle is optimized at each fixed τ angle and the rest of the molecule is constrained in a plane.

E-Z isomerization of bvpb involves the S_1 excited state.

Along the S_1 potential curve (Fig. 2), the barrier of (*E,E*)-(*E,Z*) isomerization is about seven times smaller, 0.5 eV (11.5 kcal/mol), than in the case of S_0 state, 3.17 eV (73.21 kcal/mol) showing a point at $\tau = 90^\circ$ in which the forces are not optimized because of the proximity to the TS of the S_0 potential curve, with a difference energy between them, $\Delta E_{S0\text{-}S1(90^\circ)} = 0.13$ eV (2.82 kcal/mol), and even a difference energy to that of the T_1 potential curve of $\Delta E_{S1\text{-}T1(90^\circ)} = 0.38$ eV (8.71 kcal/mol). PCM calculations (Figure S4) yield even smaller energies, with a barrier height in S_1 state of 0.4 eV (9.2 kcal/mol) and $\Delta E_{S0\text{-}S1(90^\circ)} = 0.07$ eV (1.61 kcal/mol) and $\Delta E_{S1\text{-}T1(90^\circ)} = 0.31$ eV (7.10 kcal/mol). Thus, the three electronic states, S_0, S_1 and T_1, lie almost at the same energy in the conformation of bvpb in which the vinyl group rotates $\tau = 90^\circ$, that is, this twisted conformation shows a degenerated electronic state. A similar behavior was found in other aromatic molecules such as benzene, toluene and pyrrole [56] in which the T_1 is also degenerate with the two singlet S_0 and S_1 states contributing, in some cases, to the dissociation yield under certain experimental conditions. Thus, the *E-Z* isomerization of bvpb could occur through a S_0/S_1 conical intersection (CI), as happen in most of polyene molecules [57] or *trans*-estilbene [23], and particularly in our case, an intersystem crossing to the T_1 state could be also involved, leading a *transoid*-isomer with $\tau = \pm 60^\circ$ as predicted theoretically (Fig. 2) that corresponds to a minimun in the T_1 state. This behavior is also predicted by considering PCM calculations (Figure S4). Therefore, it could be expected that bvpb molecule shows an intersystem crossing at the CI, as happen in other aromatic molecules [56]. The two S_1 and T_1 excited states of (*E,E*)-bvpb in the Franck-Condon region show the same molecular orbital type with B_u symmetry (Table S3), which correlates with B_{2u} in benzene (D_{6h} symmetry) that is basically purely biradical [58] with minimal interaction between the two unpaired electrons in the triplet. Therefore, the S_1 and T_1 states would be degenerate over the whole trajectory from the Franck-Condon region to the CI, as will be evidenced by TAS in the next section.

3.3. Femtosecond transient absorption spectra (TAS) of aqueous solution of bvpb

Fig. 3 shows the 3-D surface of the VIS-NIR time-resolved TAS of photoexcited bvpb in aqueous solution. Individual transient spectra at different delay times up to 1 ps are shown in Fig. 4. Spectra at longer delay times can be seen in Figure S5.

The VIS region (Fig. 3a, Fig. 4a) is characterized by a weak negative adsorption band in the 450–490 nm region and a strong excited state absorption (ESA) band in the 570–650 nm region with a maximum at 607 nm (2 eV). Since the S_0 state of bvpb in aqueous medium absorbs at 370 nm but the fluorescence spectrum has a strong emission band in the 390–500 nm region with a maximum at 430 nm (2.8 eV), the negative absorption band appearing in the same region is assigned to the stimulated emission (SE) originated from the locally S_1 state of the almost planar conformation. In fact, the CAM-B3LYP/6–31+G* optimization of the S_1 state for the planar (*E,E*) conformation under C_{2h} symmetry predicts an emission band at 406.5 nm in gas phase or 476.4 nm in aqueous solvent (PCM model) in agreement with the SE maximum appearing at 490 nm. A similar result is obtained for the optimized C_2 and C_i conformations of (*E,E*)-bvpb (404.7 nm, gas phase, and 474.7 nm, PCM in C_2 symmetry and 404.7 nm, gas phase, and 474.9 nm, PCM in C_i symmetry).

The VIS-TAS spectra also show in the sub-picosecond scale (Fig. 4a) that the SE band is slightly red-shifted (470 → 490 nm) while the ESA band shows a significant wavelength shift from 525 nm at 0.2 ps to 607 nm at 1 ps. This could be due to two effects: a solvation dynamic of bvpb in the S_1 state originating from the dipolar interactions with polar solvents, as shown in previous work [59,60], and even to a structural change during the vibrational relaxation process such as an internal rotation of a certain moiety with a low barrier height [61], for example the rotation of vinyl bond in S_1 state, as predicted previously by DFT calculations.

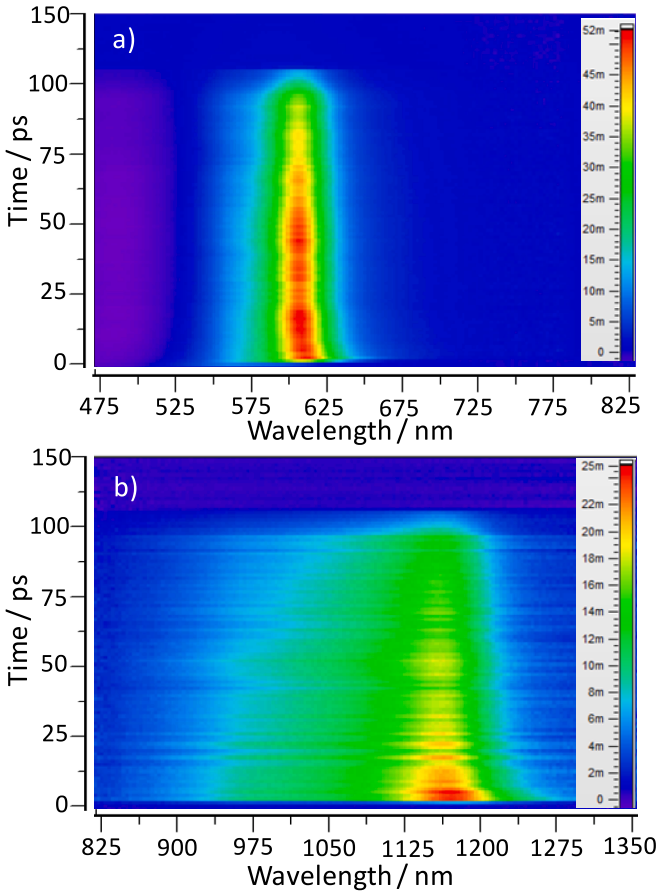

Fig. 3. Amplitude-wavelength-time (A(λ,t), ΔA(λ,t), I(λ,t)) 3-D surface of time-resolved transient absorption spectra of photoexcited bvpb in aqueous solution in the (a) VIS and (b) NIR region.

The NIR-TAS spectrum (Fig. 3b, Fig. 4b) shows a weaker broad band with a maximum at 1163 nm (1.1 eV). This indicates that the band apparent in the NIR region reflects the transition from S_1 to a higher lower state than the upper transition probed in the VIS region, that is, there is a transient species at 1.1 eV. This would correspond to a T_1 state in concordance with DFT calculation that yields an energy minimum at 0.7 eV for the T_1 state (Fig. 2). The lower absorbance signal of this band, about twice minor than that corresponding to S_1 state, is related to the spin forbidden transition S_1-T_1 and a competitive process with the S_1-S_0 allowed transition.

Figure S5 also shows the temporal profiles recorded at three selective wavelengths corresponding to SE (494 nm) and the two ESA bands (607 nm and 1163 nm) and their respective local fitting by tri-exponential functions. The three fitted lifetimes are very similar in the three bands. This feature together with the fact that both bands appear practically at the same time, that is, the 607 nm band slightly starts appearing at 260–320 fs (Fig. 4a) while the 1163 nm band begin a little after at 365–394 fs (Fig. 4b), could indicate that both S_1 and T_1 states could have a shared potential energy surface.

In the case of a global fit of VIS and NIR-TAS spectra, the dynamics of the two ESA bands were investigated by the singular value decomposition method using tri-exponential fitting functions, yielding also similar lifetimes of the three components for the two transient species. The lifetimes are: $\tau_1 = 0.46 \pm 0.42$ ps, $\tau_2 = 2.69 \pm 2.30$ ps and $\tau_3 = 72.77 \pm 8.30$ ps for the transient species at 607 nm, and $\tau_1 = 0.32 \pm 0.76$ ps, $\tau_2 = 1.71 \pm 2.10$ ps and $\tau_3 = 71.08 \pm 16$ ps for the transient species at 1163 nm.

The first component τ_1 with a domain time in the sub-picosecond

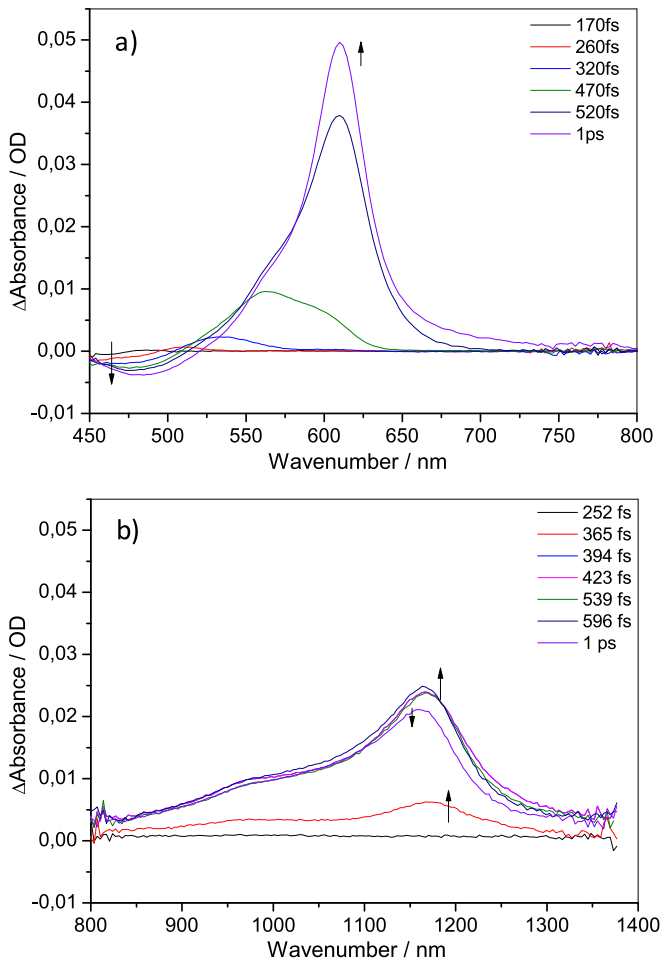

Fig. 4. Transient absorption spectra of the photoexcited bvpb in aqueous solution at different delay times below 1 ps. (a) VIS and (b) NIR region.

scale (0.46 and 0.32 ps for 607 and 1163 nm, respectively) is assignable to the vibrational relaxation and solvation effect since both processes have similar time scales in protic solvents. The photoexcitation at 370 nm (27027 cm^{-1}) populates the higher vibrational levels with about 3771.22 cm^{-1} of excess vibrational energy of the S_1 state of bvpb (emission at 430 nm = 23255.81 cm^{-1}). The growth of the SE band (Fig. 4a) is the result of vibrational relaxation in the locally planar S_1 state. The second component τ_2 (2.69 ps and 1.71 ps for 607 and 1163 nm, respectively) is assigned to the conformational relaxation, that is, the rotation around the vinyl bond as suggested by the previous work [62] and the third component, τ_3 (72.77 ps and 71.08 ps for 607 and 1163 nm, respectively) would correspond to the lifetime of S_1 and T_1 states of bvpb in aqueous medium. The shorter lifetime of both states could be correlated with the hydrogen bonding interaction between the excited state of bvpv and the aqueous solvent [63].

The similar lifetimes associated with the different relaxation processes in both S_1 and T_1 states indicate that the two states could be nearly degenerate from photoexcited states under 370 nm to CI and therefore, this is also related to a non-planar geometry for the transient species in the S_1 state. In fact, the DFT calculations (B3LYP/6–31+G*) reproduce this experimental behaviour predicting a twisted conformation of the vinylpyridyl group at $\tau = 90°$ in which the lowest singlet and triplet states, $S_{0(90°)}$ (3.16 eV), $S_{1(90°)}$ (3.29 eV) and $T_{1(90°)}$ (2.91 eV) states, are practically degenerated (Fig. 2 and Fig. S4) with a very small energy difference among them.

On the other hand, the calculated B3LYP/6–31+G* emission energies of different twisted conformations in the gas phase and aqueous solvent are smaller than the planar one (406.5 nm, gas phase; 476.4 nm, PCM), being for example those corresponding to a dihedral angle of 50° (491.7 nm, gas phase; 597.1 nm, PCM) and 60° (561.1 nm, gas phase; 689.5 nm, PCM) in the range of the experimental value of 607 nm observed in VIS-TAS spectrum. Therefore, we may conclude that the relaxation of the locally lowest excited singlet state, S_1, in aqueous solution involves the twisted vinylpyridyl group due to the lower barrier height, in order to form the phantom state [62,64] decaying equitably to the S_0 state of the *cis/trans* isomers. Absorption of new photoproducts and even the *cis*-conformer are not observed in TAS spectra due that both *trans*- and *cis*-bvpb could have practically the same UV absorption band, as expected for the stilbenes derivatives [65]. For example, an absorption band at the same region for the three isomers of bvpb is predicted by CAM-B3LYP/6–31+G* in gas phase (340 nm, 320 nm and 302 nm for the (*E,E*), (*E,Z*) and (*Z,Z*) isomers), being thus not possible to detect experimentally a TAS band of the *cis*-conformation. Even the three isomers have similar calculated Raman spectra (Figure S6) in S_0 state, yielding evidence that they are indistinguishable.

However, the analysis of electrochemical surface-enhanced Raman spectra, SERS, with the help of DFT calculations, could bring to light that a twisted conformation is involved in the SERS signal, as will discuss in the next sections.

3.4. Electrochemical SERS spectra of bvpb on a nanostructured silver electrode

Fig. 5 shows the series of electrochemical SERS spectra recorded at the 785 nm (1.58 eV) excitation line. The most interesting finding is the appearance and enhancement of two strong bands recorded at 1498 and 1154 cm^{-1} from −1.0 V up to more negative electrode potential. Other weaker bands also appear at about 1320, 1238 and 504 cm^{-1}. These bands are not recorded in SERS spectra at more positive electrode potential and not even in the Raman spectrum. In addition, the two bands at 1498 and 1154 cm^{-1} not only become the strongest ones at −1.0 V with 785 nm line (Fig. 5), but also their intensities decrease when the 532 (2.33 eV) nm line is employed and disappearing at all at 473 nm (2.59 eV) line, as can be seen in Figure S7.

The selective enhancement of certain SERS bands of aromatic molecules, is related to the presence of a chemical/charge transfer (CT) mechanism, similar to a resonant Raman process, in which excited states of different nature [29,30,43] can be involved. In many cases, photoexcited metal-to-molecule CT states of the hybrid system [31,32], or even excited state of the own adsorbate [29], are involved. Thus, SERS is a spectroscopic technique that allows getting insight into the electronic structure of a molecule adsorbed in rough metal surface and is also enable to put in evidence the presence of a resonant state, above all in electrochemical experiments in which the resonant condition can be reached with the joint action of the excitation line and the voltage. In addition, the CT states of the metal-adsorbate hybrid system, with similar characteristics to the electronic state of the radical anion [30], appear a lower energy than that of the adsorbate isolated, being possible to reach them by visible excitation line. At CAM-B3LYP/Def2TZVPP level, the first singlet excited S_1 state in bvpb isolated and the $S_1(CT_0)$ state in neutral Ag_2^0-(*E,E*)-bvpb complex is calculated at 3.65 eV (Table S3) and 2.58 eV (Table S4), respectively, being the $S_1(CT_0)$ state reachable with visible photons. In both cases, HOMO-LUMO orbitals are involved in the transition (Figure S8). Therefore, the presence of the two strong bands, 1498 and 1154 cm^{-1} at −1.0 V, could be due to the existence of a resonant process from S_0 state up to excited S_1. Due to the small barrier height of the S_1 state and the presence of a S_0/S_1 CI, the conformation of bvpb could change upon excitation from planar conformation in S_0 state to a twisted geometry corresponding to the TS or phantom state in which the vinyl bond is rotated 90°. The comparison of the calculated resonance Raman spectra between the planar Ag_2^0-(*E,E*)-bvpb and twisted geometry could shed light on this point.

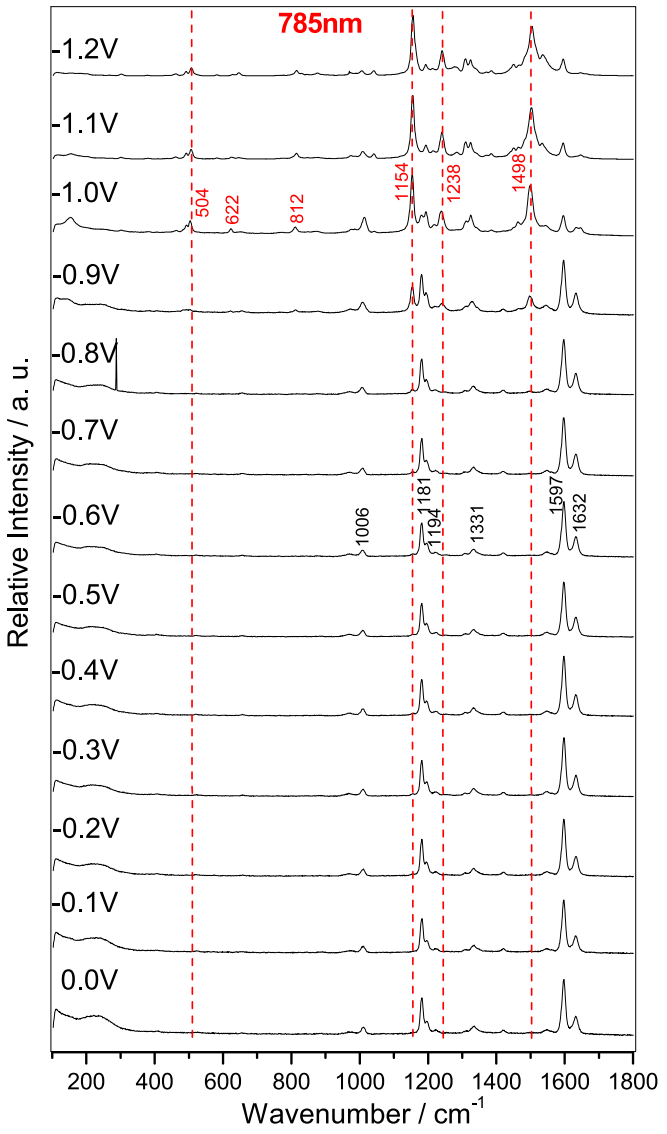

Fig. 5. Electrochemical SERS spectra of aqueous bvpb/KCl (10^{-4}M/0.1 M) solution recorded on a nanostructured silver surface in an electrode potential range from 0.0 V to −1.2 V at 785 nm excitation line.

3.5. Effect of the electrode potential on the electronic structure of bvpb adsorbed on silver surface

Interesting information can be extracted from the analysis of the linear silver-(*E,E*)-bvpb complexes, Ag_n^q-(*E,E*)-bvpb, with different sizes (n) and charges (q), used as a theoretical model to simulate the electrode potential (Figure S9).

The calculated wavenumbers (Table S5) of the neutral surface complex, Ag_2^0-(*E,E*)-bvpb, point out that all recorded SERS bands belong to in-plane totally symmetry modes. The assignment of SERS bands has been done by correlation with those reported of *E*-stilbene (Table S5 and references in Material Supplementary). Taking into account the propensity rules of the plasmonic mechanism [27], a flat or titled orientation and even reorientation of bvpb by electrode potential is discarded. Thus, bvpb adsorbs in an edge-on orientation through the nitrogen atom as happen in SERS of pyridine [31].

Also, the HOMO-LUMO gap becomes smaller at negatively charged complexes (Fig. 6). It varies from about 2 eV at positively charged complexes, concerning to an adsorbate-to-metal transition, to about 1 eV at negatively ones, where a metal-to-adsorbate transition is involved. This dual behaviour was already observed in analogue aromatic molecules [42,66]. This indicates that more negative voltage could favour the resonance process to the S_1 state. In fact, the energy of the $S_1(CT_0)$ state for each complex and the amount of charged transferred, $\Delta q = q_{Ag2}(S_i)-q_{Ag2}(S_0)$, inset of Fig. 6, confirms this evidence. While the CT_0 state remains almost constant at about 2 eV at positively charged complexes with a transferred charge of about −0.8 a.u., it drastically gets down at negatively ones reaching the lowest value, 0.01 eV, for the Ag_3^--(*E,E*)-bvpb complex with a transferred charge of 1.0 a.u. In this case, the very close proximity of the S_0 and $S_1(CT_0)$ states yields a change in the potential energy surface, appearing a new minimum that correspond to the equilibrium structure of the *cis*-conformation, Ag_3^--(*Z,E*)-bvpb. The calculated CAM-B3LYP/Def2TZVPP Raman spectra for each theoretical model (Figure S9) reproduce the SERS spectra recorded at more positive electrode potential, Figure S7, except that of Ag_3^--(*E,E*)-bvpb complex that predicts an imaginary wavenumber. It corresponds to an out-of-plane normal mode in which the vinyl torsion and the twist of pyridine ring are involved. The molecular relaxation through this normal mode drives to a *cis*-conformation, Ag_3^--(*Z,E*)-bvpb, being more stable, about 5 kcal/mol, than the corresponding all *trans*-isomer, Ag_3^--(*E,E*)-bvpb, in the S_0 state. Although the calculated Raman spectrum of Ag_3^--(*Z,E*)-bvpb complex in S_0 state (Figure S10) predicts a similar spectrum to the rest of the all-*trans* complexes, two bands in the 1600 cm^{-1} wavenumber region, the S_1 state can be reached under a red excitation line given that a vertical excitation energy of 1.53 eV is calculated (Table S4). Under resonance condition, the calculated Raman spectrum (Figure S10) is able to predict the enhancement of the three SERS bands recorded at −1.0 V, 785 nm line. Thus, these three enhanced SERS bands at −1.0 V under 785 nm line could be related to a molecular conformational change that occurs upon excitation.

3.6. Torsional potential energy curve of vinyl bond in neutral Ag_2^0-(E,E)-bvpb surface complex

The neutral complex was selected to study the torsional potential energy curve (Figure S11) because of its vertical energy (S_1 state, 2.5 eV, Table S4) is in the same order of that of bvpb isolated, as shown the TAS data (S_1 state, 2 eV (607 nm), Fig. 4). The most interesting findings are similar to those obtained for the isolated molecule, a lower barrier height in the S_1 state (1.7 eV, 49.5 Kcal/mol) than the S_0 state (3.2 eV, 73.8 Kcal/mol) and the existence of a CI in a twisted conformation with a dihedral angle of 90° at energy as much as that of isolated molecule (about 3 eV). The only difference corresponds to the equilibrium planar structure, Ag_2^0-(*E,E*)-bvpb, with a lower energy in S_1 state, 2.17 eV at CAM-B3LYP/Def2TZVPP level, than in the case of isolated bvpb, 3.38 eV at CAM-B3LYP/6–31+G* level (Fig. 2).

However, due to the presence of the silver cluster linked to one of the nitrogen atom, the two vinyl bonds become not equivalent and thus, the potential energy diagram of Ag_2^0-bvpb complex considering the rotation of the different vinyl bonds in the S_0 state was performed. The optimized structures and the minimum energies required to reach the different TS in gas phase and considering the aqueous bulk solvent are shown in Figure S12. The energy difference between the two conformers in the TS state or in the *cis*-conformation, Ag_2^0-(*E,Z*)-bvpb and Ag_2^0-(*Z,E*)-bvpb is small in both cases, about 1–2 kcal/mol. Thus, it is not possible to differentiate which C=C double bond rotates preferentially.

In any case, the Raman and resonance spectra were also calculated for those all molecular structures. The Raman spectra corresponding to the equilibrium geometry of the different optimized complexes (Figure S13) predict two intense bands in the 1600 cm^{-1} region, as happens for the isolated (*E,E*)-bvpb in S_0 state (Figure S1). Even the resonance Raman spectrum of all-*trans* bvpb, Ag_2^0-(*E,E*)-bvpb, in the S_1 state (Fig. 7) leads to the same result, the enhancement of two bands in the 1600 cm^{-1} region, and is not able to predict the new bands observed at about 1500 and 1100 cm^{-1} in the SERS spectrum at −1.0 V with 785 nm. However, the resonance spectra in the TS state (Fig. 7), that correspond to the S_0/S_1 CI surroundings, predict the enhancement of

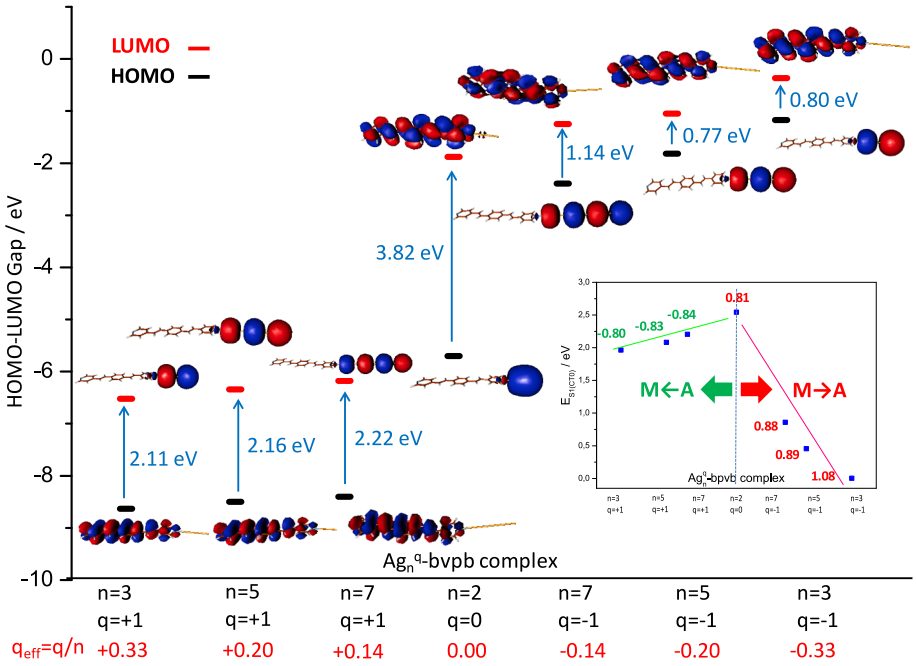

Fig. 6. HOMO-LUMO gap of the linear silver-(*E,E*)-bvpb complexes, Ag_n^q-(*E,E*)-bvpb, with different sizes (n) and charges (q) at CAM-B3LYP/Def2TZVPP level. The right inset shows the vertical energy up to the $S_1(CT_0)$ state. Red and green values correspond to the transferred charge, $\Delta q = q_{Ag2}(S_i)\text{-}q_{Ag2}(S_0)$. Positive values indicate a charge transferred from metal(M)-to-adsorbate(A). (For interpretation of the references to colour in this figure legend, the reader is referred to the web version of this article.)

three bands at about 1570, 1300 and 1180 cm^{-1} that correlate with those recorded experimentally at 1498, 1238 and 1154 cm^{-1}. This suggests that a conformational change in the structure of bvpb occurs upon excitation under resonance condition to the S_1 state, in where the twist of one of vinyl bond is mainly involved, because of their calculated spectra predict better the experimental behaviour than those with two twisted vinyl bonds. This fact also implies a significant change of the molecular distance between the free end nitrogen atom and that involved in the adsorption to silver surface (Fig. 8), working as a nanomechanical device. The vertical molecular distance is shortened from 18.30 Å in the all-*trans* Ag_2^0-(*E,E*)-bvpb at positive voltage to 13.05 or 6.49 Å at negative voltage, depending on if the end vinyl bond or the close vinyl bond to silver atom twists, respectively. Given that the S_1 state can be tuned by electrode potential, bvpb can act as a conformational switch in functionalized metal surface, being an excellent candidate for dynamic molecular machines in which it is possible to control the movement at the molecular level in a reversible manner.

4. Conclusions

The synergy of experimental femtosecond-TAS and electrochemical SERS spectra combined with DFT calculations gets insight into the *E-Z* photoisomerization process of the double heterostilbene, 1,4-bis(4-vinylpyridyl)benzene, (bvpb).

The analysis of the photoinduced excited state dynamics, by means of femtosecond-TAS, yields the presence of two transient species corresponding to the two lowest singlet ant triplet excited states, S_1 and T_1, recorded at 610 nm and 1163 nm, respectively. The tri-exponential fitting functions employed in a global fit by using the singular value decomposition method point out that three relaxation processes are involved, a vibrational relaxation and solvation dynamics in the sub-picosecond scale, the isomerization involving the rotation around the olefinic double bond in the order of 2–3 picoseconds and the electronic state decay around 70–80 picoseconds. Both S_1 and T_1 excited states show similar lifetimes associated with the different relaxation processes what implies that the two states could be nearly degenerate one each other from photoexcited states under 370 nm to CI.

The DFT results related to the potential energy curve in a hula-twist isomerization around the vinylpyridine bond shed light on this ultrafast process and point out that a S_0/S_1 conical intersection and an intersystem crossing occur at a structural conformation in which the double bond twists 90°, which could favour a degeneration of these two states, being in agreement with the experimental TAS results.

No absorption band corresponding to any *cis*-bvpb conformer is observed in TAS spectrum. Therefore, after photoexcitation of all *trans*-bvpb in the UV band, a radiation-less relaxation to the S_0 state mainly occurs through a conical intersection. In a minor proportion, other competitive deactivation process through an intersystem crossing is also involved, reaching the T_1 state that is finally deactivated by decaying to S_0 state in another radiation-less pathway, as a consequence of the collisions with the polar solvent.

The presence of the twisted conformation of bvpb has been evidenced by electrochemical SERS spectra recorded on a nanostructured silver electrode at different excitation wavelengths. The presence of two strongly enhanced bands recorded at negative voltage with 785 nm excitation line indicates that a resonance process is involved in the SERS record. From a theoretical point of view, only resonance spectra calculated for a twisted conformation at the CI point can explain this experimental feature. Therefore, SERS can be a complementary spectroscopic technique to the femtosecond-TAS for the elucidation of conformational changes in the excited states.

Furthermore, SERS experiments have shown that this twisted conformation, with a shorter N-N distance than that in the *E,E*-conformer as predicted by DFT calculations, can be tuned by the electric potential applied to the metal surface in a reversible process (forward and reverse way) without molecular damage. Therefore, a self-assembled monolayer of bvpb on metal surface holds potential as a conformational switch addressed by voltage under a selected excitation line in nanoelectronic devices. This finding would also open the way for the fabrication of new devices based on the force expressed by molecules organized in films giving a nanomotors, and towards electric switchable nanoelectronic circuits.

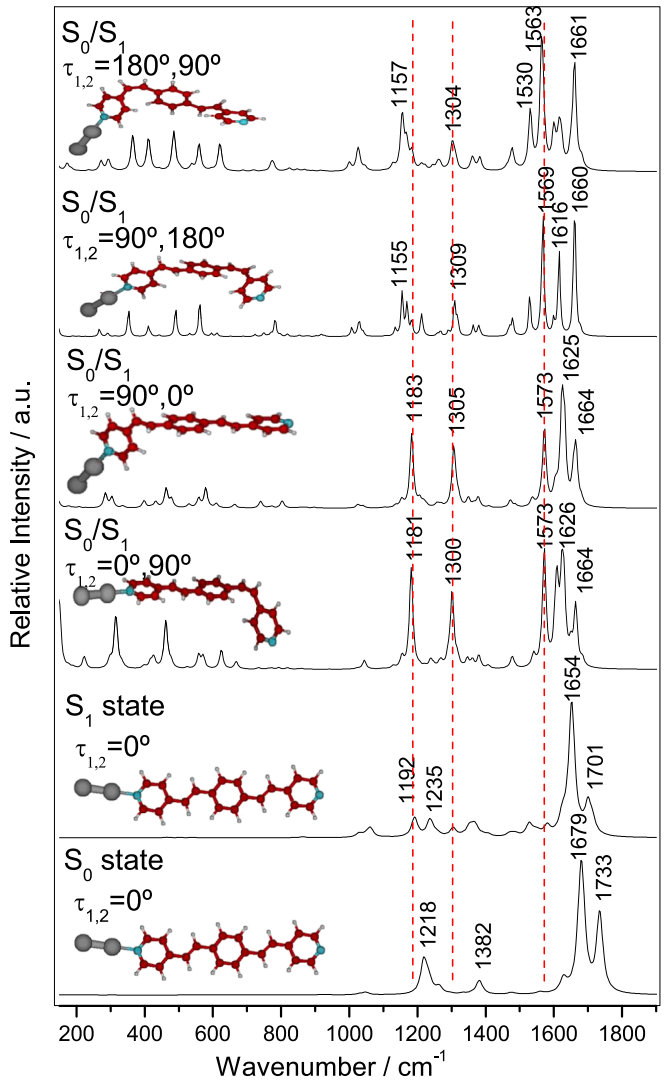

Fig. 7. TD-CAM-B3LYP/Def2TZVPP resonance Raman spectra for the Ag_2^0-(*E,E*)-bvpb complex in S_1 state and for their different conformations in the S_0/S_1 region. At the bottom, Raman spectrum of Ag_2^0-(*E,E*)-bvpb complex in the S_0 state.

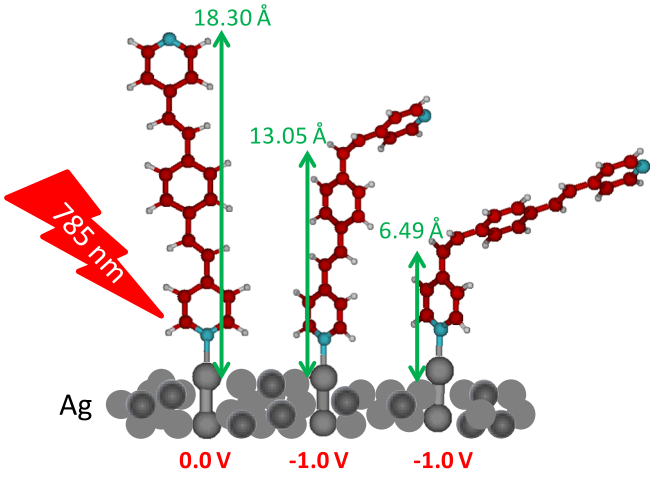

Fig. 8. Conformational changes of bvpb adsorbed on silver surface under a selected voltage and excitation wavelength.

CRediT authorship contribution statement

Isabel López-Tocón: Writing – review & editing, Writing – original draft, Methodology, Investigation, Formal analysis, Data curation, Conceptualization. **Miguel García-Castro:** Investigation. **Juan Carlos Otero:** Funding acquisition.

Declaration of competing interest

The authors declare that they have no known competing financial interests or personal relationships that could have appeared to influence the work reported in this paper.

Data availability

No data was used for the research described in the article.

Acknowledgements

This research has been supported by the Spanish Ministerio de Ciencia e Innovación/FEDER (PID2022-138559NB-I00 and PID2021-122613OB-I00) and Universidad de Málaga/FEDER (FQM-103-G-FEDER). The authors thank to the Supercomputing and Bioinnovation Center (University of Málaga) for computational resources.

Appendix A. Supplementary data

Supplementary data to this article can be found online at https://doi.org/10.1016/j.apsusc.2024.160962.

References

[1] R.S.H. Liu, D.T. Browne, A bioorganic view of the chemistry of vision: HT-n and BP-m, n mechanisms for reactions of confined, anchored polyenes, Acc. Chem. Res. 19 (1986) 42–48, https://doi.org/10.1021/ar00122a003.
[2] C.M. Pearson, T.N. Snaddon, Alkene photo-isomerization inspired by vision, ACS Cent. Sci. 3 (2017) 922–924, https://doi.org/10.1021/acscentsci.7b00376.
[3] W. Fuß, Previtamin D: Z-E photoisomerization via a Hula-twist conical intersection, Phys. Chem. Chem. Phys. 21 (2019) 6776–6789, https://doi.org/10.1039/C9CP00500E.
[4] A. Mammana, G.T. Carroll, J. Areephong, B.L. Feringa, A chiroptical photoswitchable DNA complex, J. Phys. Chem. B 115 (2011) 11581–11587, https://doi.org/10.1021/jp205893y.
[5] J. Vachon, G.T. Carroll, M.M. Pollard, E.M. Mes, A.M. Brouwer, B.L. Feringa, An ultrafast surface-bound photo-active molecular motor, Photochem. Photobiol. Sci. 13 (2014) 241–246, https://doi.org/10.1039/C3PP50208B.
[6] M. Kondo, Photomechanical materials driven by photoisomerization or photodimerization, Polym. J. 52 (2020) 1027–1034, https://doi.org/10.1038/s41428-020-0367-0.
[7] W. Fuß, C. Kosmidis, W.E. Schmid, S.A. Trushin, The photochemical cis–trans isomerization of free stilbene molecules follows a hula-twist pathway, Angew. Chem. Int. Ed. 43 (2004) 4178–4182, https://doi.org/10.1002/anie.200454221.
[8] D.H. Waldeck, Photoisomerization dynamics of stilbenes, Chem. Rev. 91 (1991) 415–436, https://doi.org/10.1021/cr00003a007.
[9] J. Qu, C.T. Cao, C. Cao, Determining the excited-state substituent constants of furyl and thienyl groups, J. Phys. Org. Chem. 31 (2018) 3799, https://doi.org/10.1002/poc.3799.
[10] M. Mlakić, L. Mandić, N. Basarić, B. Mihaljević, F. Pavošević, I. Škorić, Substituents affect the mechanism of photochemical E-Z isomerization of diarylethene triazoles via adiabatic singlet excited state pathway or via triplet excited state, J. Photchem. and Photobiol. A: Chem. 422 (2022) 113567, https://doi.org/10.1016/j.jphotochem.2021.113567.
[11] J.A. Syage, P.M. Felker, A.H. Zewail, Picosecond dynamics and photoisomerization of stilbene in supersonic beams. II. Reaction rates and potential energy surface, J. Chem. Phys. 81 (1984) 4706–4723, https://doi.org/10.1063/1.447520.
[12] J. Saltiel, A.S. Waller, D.F. Sears, Dynamics of cis-stilbene photoisomerization: the adiabatic pathway to excited trans-stilbene, J. Photochem. Photobiol. A: Chem. 65 (1992) 29–40, https://doi.org/10.1016/1010-6030(92)85029-T.
[13] W. Fuß, C. Kosmidis, W.E. Schmid, S.A. Trushin, The lifetime of the perpendicular minimum of cis-stilbene observed by dissociative intense-laser field ionization, Chem. Phys. Lett. 385 (2004) 423–430, https://doi.org/10.1016/j.cplett.2003.12.114.
[14] S.A. Kovalenko, A.L. Dobryakov, I. Ioffe, N.P. Ernsting, Evidence for the phantom state in photoinduced cis–trans isomerization of stilbene, Chem. Phys. Let. 493 (2010) 255–258, https://doi.org/10.1016/j.cplett.2010.05.022.

[15] C. Jiang, R. Xie, F. Li, R.E. Allen, Trans-to-cis isomerization of stilbene following an ultrafast laser pulse, Chem. Phys. Lett. 474 (2009) 263–267, https://doi.org/10.1016/j.cplett.2009.04.079.

[16] J.S. Baskin, L. Bañares, S. Pedersen, A.H. Zewail, Femtosecond real-time probing of reactions. 20. Dynamics of twisting, alignment, and IVR in the trans-stilbene isomerization reaction, J. Phys. Chem. 100 (1996) 11920–11933, https://doi.org/10.1021/jp960909x.

[17] M.J. Bearpark, F. Bernardi, S. Clifford, M. Olivucci, M.A. Robb, T. Vreven, Cooperating rings in cis-stilbene lead to an S0/S1 conical intersection, J. Phys. Chem. A 101 (1997) 3841–3847, https://doi.org/10.1021/jp961509c.

[18] V. Molina, M. Merchán, B.O. Roos, Theoretical study of the electronic spectrum of trans-stilbene, J. Phys. Chem. A 101 (1997) 3478–3487, https://doi.org/10.1021/jp9624109.

[19] J. Quenneville, T.J. Martínez, Ab initio study of cis−trans photoisomerization in stilbene and ethylene, J. Phys. Chem. A 107 (2003) 829–837, https://doi.org/10.1021/jp021210w.

[20] R.K. Chaudhuri, K.F. Freed, S. Chattopadhyay, U.S. Mahapatra, Theoretical studies of the ground and excited state structures of stilbene, J. Phys. Chem. A 117 (2013) 9424–9434, https://doi.org/10.1021/jp311493w.

[21] S. Pedersen, L. Bañares, A.H. Zewail, Femtosecond vibrational transition-state dynamics in a chemical reaction, J. Chem. Phys. 97 (1992) 8801–8804, https://doi.org/10.1063/1.463350.

[22] T. Baumert, T. Frohnmeyer, B. Kiefer, P. Niklaus, M. Strehle, G. Gerber, A. H. Zewail, Femtosecond transition state dynamics of cis-stilbene, Appl. Phys. B 72 (2001) 105–108, https://doi.org/10.1007/s003400000497.

[23] N. Minezawa, M.S. Gordon, Photoisomerization of stilbene: a spin-flip density functional theory approach, J. Phys. Chem. A 115 (2011) 7901–7911, https://doi.org/10.1021/jp203803a.

[24] M. Inamori, Y. Ikabata, T. Yoshikawa, H. Nakai, Unveiling controlling factors of the S/S1 minimum energy conical intersection (2): Application to penalty function method, J. Chem. Phys. 152 (2020) 144108, https://doi.org/10.1063/1.5142592.

[25] T.T. Yin, Z.X. Zhao, H.X. Zhang, Theoretical study of the cis–trans isomerization mechanism of a pendant metal-bound azobenzene, RSC Adv. 6 (2016) 79879–79889, https://doi.org/10.1039/C6RA10880F.

[26] T. Nakabayashi, H. Okamoto, M. Tasumi, Picosecond transient Raman spectra of photoexcited 4-dimethylamino-4′-nitrostilbene in polar solvents, J. Raman Spectrosc. 26 (1995) 841–845, https://doi.org/10.1002/jrs.1250260834.

[27] R. Aroca, Surface-Enhanced Vibrational Spectroscopy, John Wiley & Sons Ltd., Chichester, UK, 2006.

[28] S. Valdivia, D. Aranda, J.C. Otero, I. López-Tocón, Voltage tuning of photoinduced charge transfer resonances between 2,2′-bipyridine and a nanostructured silver electrode, Appl. Surf. Sci. 646 (2024) 158871, https://doi.org/10.1016/j.apsusc.2023.158871.

[29] I. López-Tocón, E. Imbarack, J. Soto, S. Sanchez-Cortes, P. Leyton, J.C. Otero, Intramolecular and metal-to-molecule charge transfer electronic resonances in the surface-enhanced raman scattering of 1,4-Bis((E)-2-(pyridin-4-yl)vinyl) naphthalene, Molecules 24 (2019) 4622, https://doi.org/10.3390/MOLECULES24244622.

[30] D. Aranda, S. Valdivia, F.J. Avila, J. Soto, J.C. Otero, I. López-Tocón, Charge transfer at the nanoscale and the role of the out-of-plane vibrations in the selection rules of surface-enhanced Raman scattering, Phys. Chem. Chem. Phys. 20 (2018) 29430–29439, https://doi.org/10.1039/c8cp05623d.

[31] J.F. Arenas, I. López Tocón, J.C. Otero, J.I. Marcos, Charge transfer processes in surface-enhanced raman scattering. Franck−Condon active vibrations of pyridine, J. Phys. Chem. 100 (1996) 9254–9261, https://doi.org/10.1021/jp953712y.

[32] J.F. Arenas, M.S. Woolley, I. López Tocón, J.C. Otero, J.I. Marcos, Complete analysis of the surface-enhanced Raman scattering of pyrazine on the silver electrode on the basis of a resonant charge transfer mechanism involving three states, J. Chem. Phys. 112 (2000) 7669–7683, https://doi.org/10.1063/1.481361.

[33] L. Liao, X. Zhang, F. Hu, S. Wang, S. Xu, Q. Zeng, C. Wang, Two-Dimensional supramolecular self-assembly of stilbene derivatives with ester groups: molecular symmetry and alkoxy substitution effect, J. Phys. Chem. C 118 (2014) 7989–7995, https://doi.org/10.1021/jp412793w.

[34] N.K. Annan, P.R. Cook, S.T. Mullins, G. Lowe, Evidence for cross-linking DNA by bis-intercalators with rigid and extended linkers is provided by knotting and catenation, Nucleic Acids Res. 20 (1992) 983–990, https://doi.org/10.1093/nar/20.5.983.

[35] R.G. Parr, W. Yang, Density-Functional Theory of Atoms and Molecules, Oxford University Press, New York, 1989.

[36] A.D. Becke, Density-functional thermochemistry. III. The role of exact exchange, J. Chem. Phys. 98 (1993) 5648–5652, https://doi.org/10.1063/1.464913.

[37] J.-D. Chai, M. Head-Gordon, Systematic optimization of long-range corrected hybrid density functionals, J. Chem. Phys. 128 (2008) 084106, https://doi.org/10.1063/1.2834918.

[38] T. Yanai, D. Tew, N. Handy, A new hybrid exchange-correlation functional using the Coulomb-attenuating method (CAM-B3LYP), Chem. Phys. Lett. 393 (2004) 51–57, https://doi.org/10.1016/j.cplett.2004.06.011.

[39] G.A. Petersson, M.A. Al-Laham, A complete basis set model chemistry. II. Open-shell systems and the total energies of the first-row atoms, J. Chem. Phys. 94 (1991) 6081–6090, https://doi.org/10.1063/1.460447.

[40] F. Weigend, R. Ahlrichs, Balanced basis sets of split valence, triple zeta valence and quadruple zeta valence quality for H to Rn: design and assessment of accuracy, Phys. Chem. Chem. Phys. 7 (2005) 3297–3305, https://doi.org/10.1039/B508541A.

[41] F. Avila, D.J. Fernandez, J.F. Arenas, J.C. Otero, J. Soto, Modelling the effect of the electrode potential on the metal–adsorbate surface states: relevant states in the charge transfer mechanism of SERS, Chem. Commun. 47 (2011) 4210–4212, https://doi.org/10.1039/c0cc05313a.

[42] S. Valdivia, F.J. Avila, J.C. Otero, I. López-Tocón, Voltage selection of physisorbed or chemisorbed 4-cyanobenzoate on a nanostructured silver electrode and the dual electronic structure of charged metal–molecule hybrids, Appl. Surf. Sci. 579 (2022) 152071, https://doi.org/10.1016/j.apsusc.2021.152071.

[43] M.L. de Souza, S. Valdivia, J.C. Otero, I. López-Tocón, Sensing bisphenol a by means of surface-enhanced raman spectroscopy and DFT calculations to elucidate the enhancement mechanism that dominates the spectrum, Chemosensors 11 (2023) 78, https://doi.org/10.3390/chemosensors11020078.

[44] D.A. Long, The raman effect: a unified treatment of the theory of raman scattering by molecules, Wiley, 2002.

[45] J. Neugebauer, M. Reiher, C. Kind, B.A. Hess, Quantum chemical calculation of vibrational spectra of large molecules Raman and IR spectra for Buckminsterfullerene, J. Comput. Chem. 23 (2002) 895–910, https://doi.org/10.1002/jcc.10089.

[46] G. Schaftenaar, J.H. Noordik, Molden: a pre- and post-processing program for molecular and electronic structures, J. Comp.-Aided Mol. Design 14 (2000) 123–134, https://doi.org/10.1023/A:1008193805436.

[47] M. J. Frisch, G. W. Trucks, H. B. Schlegel, G. E. Scuseria et al., Gaussian 16 Rev. C.02., Inc., Wallingford CT, 2019.

[48] J. Bernstein, Refinement of trans-stilbene: a comparison of two crystallographic studies, Acta Cryst B31 (1975) 1268–1271, https://doi.org/10.1107/S0567740875005031.

[49] O. Lhost, J.L. Brédas, Theoretical study of torsion potentials in trans-stilbene and substituted trans-stilbenes: modelling torsions in ploy(paraphenylene vinylene) and derivatives, J. Chem. Phys. 96 (1992) 5279–5288, https://doi.org/10.1063/1.462713.

[50] M. Traetteberg, E.B. Frantsen, F.C. Mijlhoff, A. Hoekstra, A gas electron diffraction study of the molecular structure of trans-stilbene, J. Mol. Struct. 26 (1975) 57–68, https://doi.org/10.1016/0022-2860(75)80066-4.

[51] J.A. Bouwstra, A. Schouten, J. Kroon, Structural studies of the system trans-azobenzene/trans-stilbene. II. A reinvestigation of the disorder in the crystal structure of trans-stilbene, $C_{14}H_{12}$, Acta Cryst. C 40 (1984) 428–431, https://doi.org/10.1107/S010827018400439X.

[52] J.R. Ackerman, B.E. Kohler, s-cis octatetraene: ground state barrier for s-cis to s-trans isomerization, J. Chem. Phys. 81 (1984) 45–50, https://doi.org/10.1063/1.446470.

[53] J.P. Aime, F. Bargain, M. Schott, H. Eckhardt, G.G. Miller, R.L. Elsenbaumer, Structural study of doped and undoped polythiophene in solution by small-angle neutron scattering, Phys. Rev. Lett. 62 (1989) 55, https://doi.org/10.1103/PhysRevLett.62.55.

[54] A.M. Müller, S. Lochbrunner, W.E. Schmid, W. Fuß, Low-temperature photochemistry of previtamin D: a hula-twist isomerization of a triene, Angew. Chem. Int. Ed. 37 (1998) 505–507, https://doi.org/10.1002/(SICI)1521-3773(19980302)37:4<505::AID-ANIE505>3.0.CO;2-U.

[55] The case of medium-dependent dual mechanisms for photoisomerization: one-bond-flip and hula-twist. Proc. Natl. Acad. Sci. USA 97 (2000) 11153-11158, DOI: 10.1073/pnas.210323197.

[56] S. Cogan, Y. Haas, S. Zilberg, Intersystem crossing at singlet conical intersections, J. Photochem. and Photobiol. A: Chemistry 190 (2007) 200–206, https://doi.org/10.1016/j.jphotochem.2007.02.005.

[57] P. Celani, M. Garavelli, S. Ottani, F. Bernardi, M.A. Robb, M. Olivucci, Molecular" trigger" for the radiationless deactivation of photoexcited conjugated hydrocarbons, J. Am. Chem. Soc. 117 (1995) 11584–11585, https://doi.org/10.1021/ja00151a026.

[58] L. Salem, C. Rowland, The electronic properties of diradicals, Angew. Chem. Int. Ed. 11 (1972) 92–111, https://doi.org/10.1002/anie.197200921.

[59] Y. Wu, W. Zhu, Organic sensitizers from D–π–A to D-A–π–A: effect of the internal electron-withdrawing units on molecular absorption, energy levels and photovoltaic performances, Chem. Soc. Re. 42 (2013) 2039–2058, https://doi.org/10.1039/C2CS35346F.

[60] S.A. Kovalenko, N. Eilers-König, T.A. Senyushkina, N.P. Ernsting, Charge transfer and solvation of betaine-30 in polar solvents a femtosecond broadband transient absorption study, J. Phys. Chem. A 105 (2001) 4834–4843, https://doi.org/10.1021/jp004007e.

[61] S. Lee, M. Jen, T. Jang, G. Lee, Y. Pang, Twisted intramolecular charge transfer of nitroaromatic push-pull chromophores, Sci Rep. 12 (2022) 6557, https://doi.org/10.1038/s41598-022-10565-6.

[62] O. Jean, J. Gediminas, A. Emmanuel, L. René, R. Claude, Time-resolved charge transfer in "Push-Pull" stilbenes, Bull. Chem. Soc. Jpn. 75 (2002) 1041–1047, https://doi.org/10.1246/bcsj.75.1041.

[63] S. Hirai, M. Banno, K. Ohta, D.K. Palit, K. Tominaga, Vibrational dynamics of the CO stretching mode of 9-fluorenone in alcohol solution, Chem. Phys. Lett. 450 (2007) 44–48, https://doi.org/10.1016/j.cplett.2007.10.090.

[64] H. Gruen, H. Goerner, Trans-cis photoisomerization, fluorescence, and relaxation phenomena of trans-4-nitro-4'-(dialkylamino)stilbenes and analogues with a nonrotatable amino group, J. Phys. Chem. 93 (1989) 7144–7152, https://doi.org/10.1021/j100357a024.

[65] R.N. Beale, E.M.F. Roe, Ultra-violet absorption spectra of trans- and cis-stilbenes and their derivatives. Part I. Trans- and cis-Stilbenes, J. Chem. Soc. (Resumed) (1953) 2755–2763.

[66] J. Roman-Perez, S.P. Centeno, M.R. López-Ramírez, J.F. Arenas, J. Soto, I. López-Tocón, J.C. Otero, On the dual character of charged metal–molecule hybrids and the opposite behaviour of the forward and reverse CT processes, Phys. Chem. Chem. Phys. 16 (2014) 22958–22961, https://doi.org/10.1039/c4cp03984j.